ACS APPLIED MATERIALS & INTERFACES

Research Article

Cite This: ACS Appl. Mater. Interfaces 2020, 12, 494−506

www.acsami.org

High Performance Na-O_2 Batteries and Printed Microsupercapacitors Based on Water-Processable, Biomolecule-Assisted Anodic Graphene

Jose M. Munuera,*[,†,‡] Juan I. Paredes,*[,†] Marina Enterría,[§] Silvia Villar-Rodil,[†] Adam G. Kelly,[‡] Yashaswi Nalawade,[‡] Jonathan N. Coleman,[‡] Teófilo Rojo,[§,∥] Nagore Ortiz-Vitoriano,[§,⊥] Amelia Martínez-Alonso,[†] and Juan M. D. Tascón[†]

[†]Instituto Nacional del Carbón, INCAR-CSIC, C/Francisco Pintado Fe 26, 33011 Oviedo, Spain

[‡]School of Physics and CRANN, Trinity College Dublin, Pearse St, Dublin 2, Dublin D02, Ireland

[§]CIC EnergiGUNE, Álava Technology Park, C/ Albert Einstein 48, Miñano, Álava 01510, Spain

[∥]Departamento de Química Inorgánica, Universidad del País Vasco UPV/EHU, P.O. Box 664, 48080 Bilbao, Spain

[⊥]IKERBASQUE, Basque Foundation for Science, 48013 Bilbao, Spain

Supporting Information

ABSTRACT: Integrated approaches that expedite the production and processing of graphene into useful structures and devices, particularly through simple and environmentally friendly strategies, are highly desirable in the efforts to implement this two-dimensional material in state-of-the-art electrochemical energy storage technologies. Here, we introduce natural nucleotides (e.g., adenosine monophosphate) as bifunctional agents for the electrochemical exfoliation and dispersion of graphene nanosheets in water. Acting both as exfoliating electrolytes and colloidal stabilizers, these biomolecules facilitated access to aqueous graphene bio-inks that could be readily processed into aerogels and inkjet-printed interdigitated patterns. Na-O_2 batteries assembled with the graphene-derived aerogels as the cathode and a glyme-based electrolyte exhibited a full discharge capacity of ∼3.8 mAh cm^{-2} at a current density of 0.2 mA cm^{-2}. Moreover, shallow cycling experiments (0.5 mAh cm^{-2}) boasted a capacity retention of 94% after 50 cycles, which outperformed the cycle life of prior graphene-based cathodes for this type of battery. The positive effect of the nucleotide-adsorbed nanosheets on the battery performance is discussed and related to the presence of the phosphate group in these biomolecules. Microsupercapacitors made from the interdigitated graphene patterns as the electrodes also displayed a competitive performance, affording areal and volumetric energy densities of 0.03 μWh cm^{-2} and 1.2 mWh cm^{-3} at power densities of 0.003 mW cm^{-2} and 0.1 W cm^{-3}, respectively. Taken together, by offering a green and straightforward route to different types of functional graphene-based materials, the present results are expected to ease the development of novel energy storage technologies that exploit the attractions of graphene.

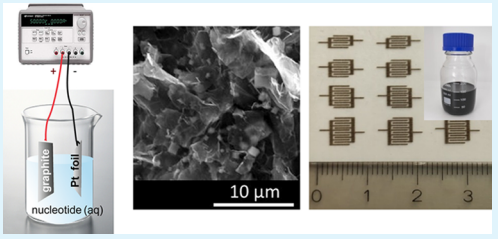

KEYWORDS: *graphene, electrochemical exfoliation, biomolecule, metal-oxygen batteries, microsupercapacitors*

1. INTRODUCTION

Over the last decade, extensive research efforts have been devoted worldwide to explore the potential of graphene and its derivatives in energy storage applications, particularly electrochemical energy storage (EES) as a very promising technology in the efforts to tackle the current energy and environmental crisis.[1−3] Boasting many attractive features, including large surface area, good mechanical and chemical stabilities, as well as high electrical conductivity, graphene is considered an excellent candidate as an electrode component in different types of batteries (metal-ion, metal-air, metal-sulfur, etc.)[1−4] and supercapacitors (both conventional and small-scale devices).[2,3,5] As regards the former type of EES device, it is worth noting that current metal-ion batteries have reached their limits in terms of theoretical energy density, cycle life, and charge/discharge rate, and so, the development of a sustainable energy grid requires the implementation of new generations of batteries with enhanced features. In this context, metal-air (M-O_2) batteries have arisen as an attractive alternative to conventional batteries due to their high theoretical energy density.[6,7] In particular, Na-O_2 batteries exhibit important advantages, including wide availability of Na metal, lower overpotential during charge, and high coulombic efficiency.[8] Unlike conventional metal-ion batteries, solid discharge products are generated during the cycling of Na-O_2 batteries, with sodium superoxide (NaO_2) being the most interesting product owing to its reversible formation. Nevertheless, a number of issues, such as the uncontrollable generation of

Received: August 28, 2019
Accepted: December 11, 2019
Published: December 11, 2019

DOI: 10.1021/acsami.9b15509
ACS Appl. Mater. Interfaces 2020, 12, 494−506

parasitic products or a limited reversibility, hinder at present the prospects of these devices to replace metal-ion batteries. Concerning supercapacitors, a current focus is placed on the development of miniaturized systems, that is, microsupercapacitors, for use as power sources in flexible and wearable electronics.[5,9] In this case, planar devices with good performance can be conveniently prepared from inks that incorporate the active electrode material (e.g., graphene) or other device components by using well-established (inkjet, screen, gravure, etc.) printing techniques.[9] However, ink formulation is frequently a complicated process where non-innocuous additives and organic solvents are used instead of water, even though the latter would ideally be the medium of choice for practical and economic reasons.

It is clear that fulfilling the expectations placed on graphene in these EES applications will rely on the availability of competitive methods (i.e., methods that are simple, versatile and cost-effective) for the production and processing of graphene-based materials with final characteristics that are specifically targeted to each intended use. Moreover, in a world plagued by pressing environmental and sustainability issues, the development of green, environmentally friendly (e.g., bio-based) graphene manufacturing strategies should be given preference.[10,11] For example, with a view to its use as a cathode in M-O_2 batteries, processing graphene into suitable three-dimensional porous architectures having well-interconnected nanosheets is expected to be advantageous since an efficient electron transport, unimpeded access of ions and gas molecules as well as proper accommodation of the discharge products throughout the electrode can be simultaneously attained with such architectures.[4,12] These requirements can in principle be met by using graphene foams or aerogels obtained by chemical vapor deposition (CVD) techniques that employ metal (e.g., Ni) foams acting both as a catalyst and template.[4,13,14] Unfortunately, the high temperatures and controlled synthesis atmospheres usually associated to such techniques, together with the need to remove the metal template after the synthesis step, make the CVD approach expensive and difficult to scale up. Instead, graphene oxide (GO) is commonly used as a starting material for the preparation of graphene-based foams/aerogels by different wet techniques, owing to its good processability in water and a number of polar organic solvents.[4,14,15] Nonetheless, even though single-layer GO nanosheets can be obtained in very high yields through well-established protocols, their production generally involves the use of harsh reagents (strong acids and oxidants), and a built-in or post-synthesis reduction step must be incorporated to make the resulting three-dimensional structure electrically conductive. Likewise, having nanosheets colloidally dispersed in the liquid phase in the form of stable and concentrated inks provides access to graphene-based printed microsupercapacitors.[5,9] In this case, GO is also a frequent material of choice, its use suffering again from the abovementioned drawbacks. Resorting to pristine graphene-based inks prepared through direct, ultrasound- or shear force-induced delamination of graphite can be a possible way out,[9,16] but these strategies are generally associated to low exfoliation yields (typically below 5 wt %) and degrees (relatively thick nanosheets).[17]

On the other hand, the electrochemical exfoliation of graphite, particularly under anodic conditions, has recently emerged as an attractive alternative for the production of graphene nanosheets toward different energy-related applications.[18−20] There are a number of assets associated to this method, including simplicity of operation, alacrity, scalability, versatility in the selection of electrolytes, ability to deliver high exfoliation yields and degrees, as well as the possibility to control the oxidation extent of the exfoliated nanosheets in a broad range (from almost no oxidation to levels typical of GO).[21−23] However, to facilitate the development of different types of electrode architectures for EES devices and other applications, the electrochemically exfoliated graphene nanosheets need to be processed in the liquid phase and particularly in water for safety and sustainability reasons. Furthermore, integrated approaches that allow the electrochemical exfoliation and colloidal dispersion of graphene in an aqueous medium using the minimum number of (preferably green) reagents (electrolytes, surfactants, etc.) and processing steps would also be highly desirable on practical and economic grounds, but they have seldom been reported (and never toward energy-related applications).[24,25]

Here, we introduce such an approach by resorting to small, innocuous biomolecules that exhibit a dual functionality. Specifically, we show that selected natural nucleotides can be used in the dual role of exfoliating electrolyte and colloidal stabilizer for the preparation and dispersion of electrochemically exfoliated graphene in water. Moreover, aerogels and inkjet-printed interdigitated patterns have been obtained from the aqueous graphene bio-ink that results from this green, straightforward exfoliation/dispersion process. Significantly, Na-O_2 batteries assembled with the graphene aerogels as the cathode and a glyme-based electrolyte outperformed previously reported graphene-based cathodes in terms of cycle life, a critical parameter in the development of this novel type of battery, and the interdigitated graphene patterns were successfully used as electrodes for microsupercapacitors. Overall, by introducing a particularly simple, efficient, and economic production strategy that can be easily integrated with further processing steps, the present work should expedite the widespread adoption of graphene-based materials in state-of-the-art EES technologies.

2. RESULTS AND DISCUSSION

2.1. Electrochemical Exfoliation and Dispersion of Graphene in Water with Bifunctional Nucleotides. The electrochemical exfoliation of graphite in water to give graphene nanosheets is usually carried out under anodic conditions using inorganic acids (mostly H_2SO_4) or their salts [$(NH_4)_2SO_4$, Na_2SO_4, etc.] as the electrolyte.[18,19,26−29] Under such conditions, an efficient delamination of the graphite anode is generally accomplished so that graphene is obtained in considerable yields and with a good exfoliation degree (single to a few layer nanosheets). Nevertheless, even though the resulting products are subjected to extensive washing, remnants of the electrolyte are likely to be retained on the nanosheets, which could negatively impact their characteristics (colloidal stability, adsorption capacity, etc.). Furthermore, unless they are produced in a highly oxidized form (similar to GO),[23] the anodic graphene nanosheets are directly dispersible only in certain organic solvents (e.g., *N*,*N*-dimethylformamide) but not in water, even though the latter is the preferable solvent for practical, economic, and sustainability reasons. Thus, the use of proper stabilizing agents becomes necessary to disperse and process anodic graphene in an aqueous medium, with surfactants of synthetic origin being the most widely available stabilizers,[17] In this context, the ability to anodically exfoliate and colloidally disperse graphene nanosheets in water

DOI: 10.1021/acsami.9b15509
ACS Appl. Mater. Interfaces 2020, 12, 494−506

by resorting to a single compound, ideally of natural origin, that acted both as an exfoliating electrolyte and stabilizer is highly desirable. To this end, we turned our attention to RNA/DNA-related and other nucleotides. Being made up of a hydrophobic heterocyclic base (nucleobase) connected to a hydrophilic phosphorylated sugar moiety,[30] nucleotides are intrinsically amphiphilic molecules that can play the role of a colloidal stabilizer for graphene and other carbon nanostructures in water.[31,32] Furthermore, owing to their anionic character afforded by the phosphate group, nucleotides could be exploited as an electrolyte for the intercalation and exfoliation of graphite in anodic processes.

For the electrochemical exfoliation experiments, we selected the RNA-related nucleotides adenosine monophosphate (AMP), guanosine monophosphate (GMP), and adenosine triphosphate (ATP) as well as flavin mononucleotide (FMN), all of them in their sodium salt form. The chemical structures of these nucleotides are shown in Figure 1. Graphite foil (a modestly priced, widely available type of graphite) and a platinum foil were used as the anode and cathode, respectively, of an electrolytic cell that contained an aqueous solution of a given nucleotide (see the Experimental Section for details and Figure 2a for a schematic representation of the electrolytic setup). Upon application of a positive voltage (typically +10 V) to the graphite foil in the presence of proper concentrations of the nucleotides (0.01−0.5 M), the anode was seen to progressively swell in the course of several minutes, thus providing a first indication of the successful intercalation and expansion of the graphitic material. This point is illustrated in Figure 2b, which shows digital photographs of a graphite foil piece before (left) and after (right) electrolytic treatment in 0.1 M AMP for 60 min. Further inspection of the nucleotide-expanded material by scanning electron microscopy (SEM) revealed it to be made up of long, accordion-shaped particles (Figure 2c), which in turn displayed a morphology of very thin, wrinkled, or rippled sheets separated by micrometer- or submicrometer-sized voids (Figure 2d). Such a morphology is known to be a characteristic of efficient processes of anodic delamination of graphite with common aqueous electrolytes (e.g., sulfate-based),[27,29,33] thereby suggesting that the present nucleotides are also good exfoliating electrolytes for the attainment of graphene nanosheets.

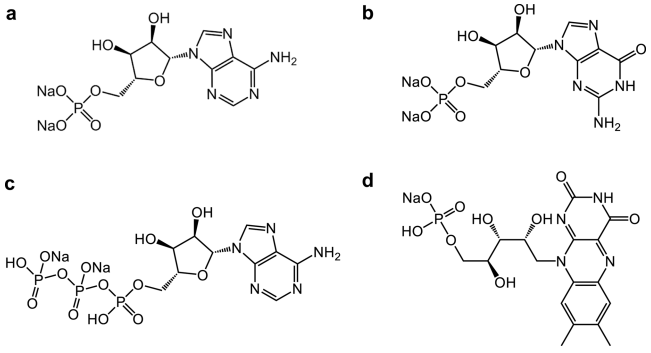

Figure 1. Chemical structure of the disodium salts of (a) adenosine 5′-monophosphate (AMP), (b) guanosine 5′-monophosphate (GMP), (c) adenosine 5′-triphosphate (ATP) as well as (d) flavin 5′-monophosphate FMN.

In addition to their natural origin and innocuity, one significant advantage of the nucleotides over conventional electrolytes is their suitability as dispersing agents to colloidally stabilize the exfoliated nanosheets in the aqueous electrolytic medium itself, which facilitated their subsequent processing into different materials. After the anodic treatment, the wet-expanded material was gently scraped off the graphite foil electrode with a spatula, directly poured into the electrolytic solution, and bath-sonicated for 3 h to extract and disperse individual graphene nanosheets. The sonicated dispersion was then subjected to a washing protocol that included a high-speed centrifugation step to completely sediment the material, followed by redispersion of the sediment in pure water with the

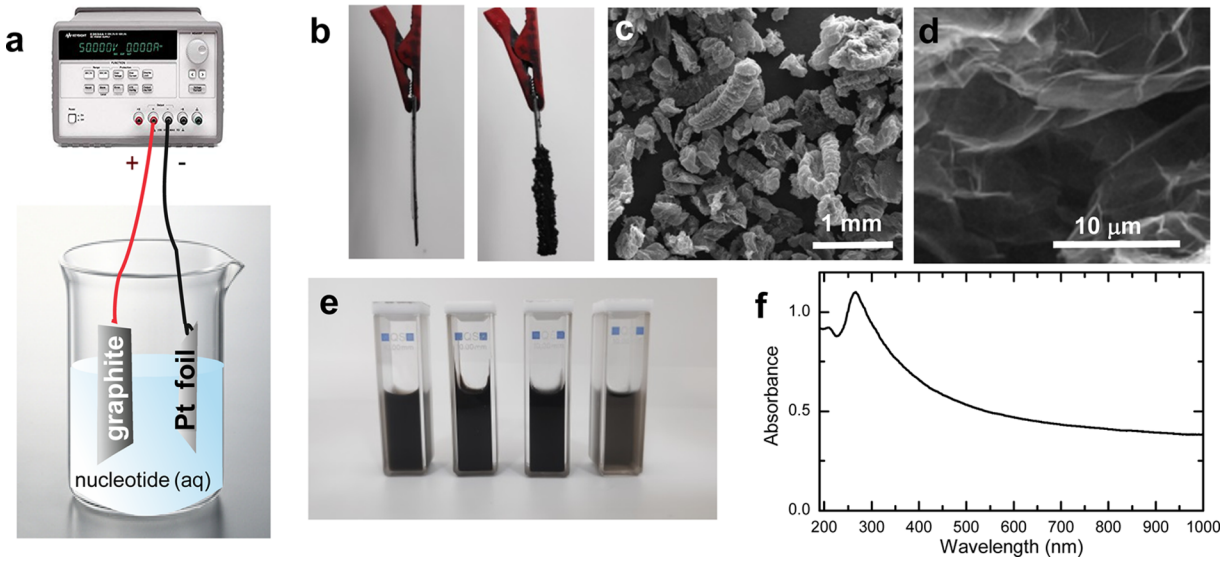

Figure 2. (a) Schematic of the electrochemical exfoliation of graphite using an aqueous solution of a given nucleotide (AMP, GMP, ATP, or FMN) as the electrolytic medium. (b) Digital photographs of a graphite foil piece before (left) and after (right) electrolytic treatment in 0.1 M AMP for 60 min. (c, d) Representative FE-SEM images of the electrochemically expanded graphite piece at (c) low and (d) high magnification. (e) Digital photograph of graphene aqueous suspensions extracted by ultrasound treatment from the material expanded in 0.1 M aqueous solutions of (from left to right): AMP, GMP, ATP, and FMN. (f) UV−vis absorption spectrum of AMP-derived graphene suspension in water.

DOI: 10.1021/acsami.9b15509
ACS Appl. Mater. Interfaces 2020, 12, 494−506

aid of a brief sonication, and finally low-speed centrifugation to separate poorly delaminated components from the well-exfoliated nanosheets retained in the supernatant (see the Experimental Section for protocol details). Figure 2e shows a digital photograph of the resulting, opaque black aqueous dispersions obtained with the different nucleotides in 0.1 M electrolytic solutions. The dispersions were generally seen to remain colloidally stable and homogeneous for weeks, showing little or no visual sign of precipitation. By contrast, hardly any suspended material could be attained when the electrochemically expanded product was processed in pure water rather than the electrolytic solution, thus highlighting the bifunctional role of the nucleotides as exfoliating electrolytes and stabilizers.

The nucleotide-derived dispersions exhibited a dominant optical absorption peak at a wavelength of ~270 nm in combination with strong absorption at longer wavelengths, as exemplified in the UV−vis absorption spectrum of an AMP-derived sample shown in Figure 2f. These features are known to be a characteristic of graphene materials having limited extents of oxidation, including pristine graphene and highly reduced GO.[34,35] The weak absorption peak noticed in Figure 2f at ~210 nm could be ascribed to the AMP molecules present in the dispersion as a stabilizer.[36] The UV−vis absorption spectra were used to estimate the concentration of dispersed materials in the suspensions on the basis of the Lambert−Beer law,[32] which in turn was taken as a measure of the overall efficiency of the nucleotides in the combined anodic exfoliation/dispersion process. As could be anticipated, the dispersed graphene concentration tended to increase with increasing concentration of the starting nucleotide solution in the tested range between 0.01 and 0.5 M. However, for AMP, GMP, and FMN, an optimum electrolyte concentration of ~0.1 M was determined. Above this threshold, increasing the electrolyte concentration did not result in changes in the dispersed graphene concentration of equal magnitude (e.g., doubling the nucleotide concentration from 0.1 to 0.2 M did not allow doubling the dispersed graphene concentration). For ATP, a lower optimum concentration was ascertained (~0.05 M). Such a result was likely related to a higher efficiency of this nucleotide in its role as an exfoliating electrolyte and/or dispersant, which in turn would be induced by its larger negative charge compared to that of the other nucleotides.[24,37]

Using the optimum electrolyte concentrations, aqueous suspensions with graphene concentrations of ~0.5−0.7 mg mL^{-1} were typically achieved, which translated into overall yields of the combined exfoliation/dispersion process, defined as the total amount of dispersed graphene relative to the initial weight of the graphite foil electrode, of about 40−50 wt % for ~100 μm thick foils. These figures were comparable to prior graphene yields reported for the anodic exfoliation of graphite foil of similar thickness with common electrolytes,[27,38,39] thus demonstrating the high efficacy of the nucleotides in their dual role as an exfoliating electrolyte and dispersant. As could be expected, the graphene yield was strongly dependent on the thickness of the graphite foil, larger thicknesses leading to lower yields (e.g., a yield of ~5−10 wt % was determined for ~500 μm thick foils). Nevertheless, the efficiency of the whole process could be increased by reusing both the original electrolytic solution and the remaining (nonexpanded) fraction of the graphite foil electrode in subsequent anodic exfoliation/dispersion cycles. The nucleotide solution was reclaimed during purification of the anodically expanded and sonicated material, and although its concentration should be somewhat lower than that of the starting fresh solution (a small fraction of the nucleotide molecules were transferred to the graphene dispersion), it was still sufficient to afford a few additional processing cycles. We also note that more concentrated graphene suspensions (e.g., 2−3 mg mL^{-1}) could be readily obtained from the as-prepared, nucleotide-stabilized dispersions by subjecting the latter to consecutive cycles of sedimentation via centrifugation and redispersion in smaller aqueous volumes. As described below, these concentrated suspensions or bio-inks (see Figure S1 in the Supporting Information) could be readily processed into different graphene-based materials (aerogels, inkjet-printed patterns) for use in different applications.

The nature of the anodically delaminated and colloidally dispersed materials as graphene nanosheets of a good structural quality was confirmed by different microscopic and spectroscopic techniques. Scanning transmission electron microscopy (STEM) images (Figure 3a,b) revealed that the dispersed

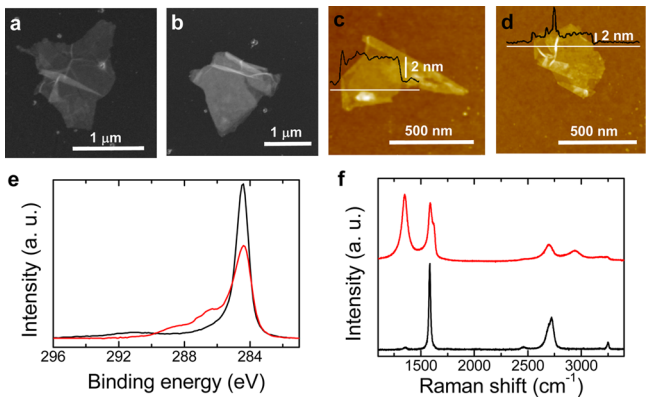

Figure 3. Microscopic and spectroscopic characterizations of graphene nanosheets extracted by sonication in water from graphite anodically expanded using 0.1 M AMP. (a, b) STEM and (c, d) AFM images of graphene nanosheets. Typical line profiles of the nanosheets (black traces) taken along the marked white lines are shown overlaid on the AFM images. (e) Background-subtracted, high resolution XPS C1s core level spectrum of the starting graphite foil (black trace) and the graphene nanosheets obtained from graphite anodically expanded using 0.1 M AMP. (f) Raman spectra of anodic graphene obtained with 0.1 M AMP (red trace) and the starting graphite (black trace).

objects consisted of flakes with irregular polygonal shapes and typical lateral sizes between a few and several hundreds of nanometers. This conclusion was corroborated by atomic force microscopy (AFM), as illustrated in Figure 3c,d for flakes deposited onto SiO_2/Si, where they were seen to be decorated by globular features ~1−2 nm high that were ascribed to adsorbed nucleotide molecules. Indeed, the density of globules tended to decrease when the nanosheets were subjected to washing protocols to remove the nucleotides (e.g., repeated cycles of sedimentation and redispersion in pure water). Line profiles taken from the AFM images across globule-free areas indicated the apparent thickness of the nanosheets to be ~1.5−2.5 nm. Considering that AFM images of different types of graphene (both pristine and oxidized) supported onto SiO_2/Si substrates incorporate a positive height offset of about 1 nm,[40,41] the actual thickness of the present nanosheets could be estimated as ~0.5−1.5 nm, implying a dominance of few-layered (≤5) objects. Transmission electron microscopy (TEM) images of representative few-layer (≤ 5) graphene

DOI: 10.1021/acsami.9b15509
ACS Appl. Mater. Interfaces 2020, 12, 494−506

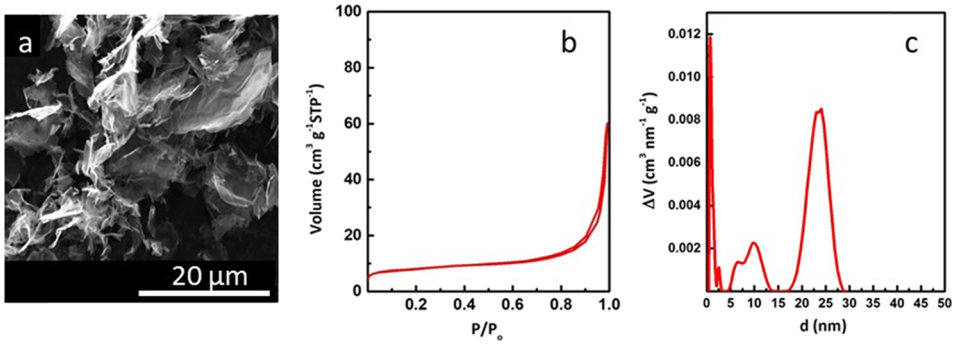

Figure 4. (a) SEM image, (b) nitrogen adsorption/desorption isotherm of a graphene aerogel prepared by freeze-drying an aqueous suspension of graphene nanosheets obtained through anodic exfoliation and dispersion with 0.1 M AMP, and (c) PSD calculated from the isotherm by the 2D-NLDFT method.

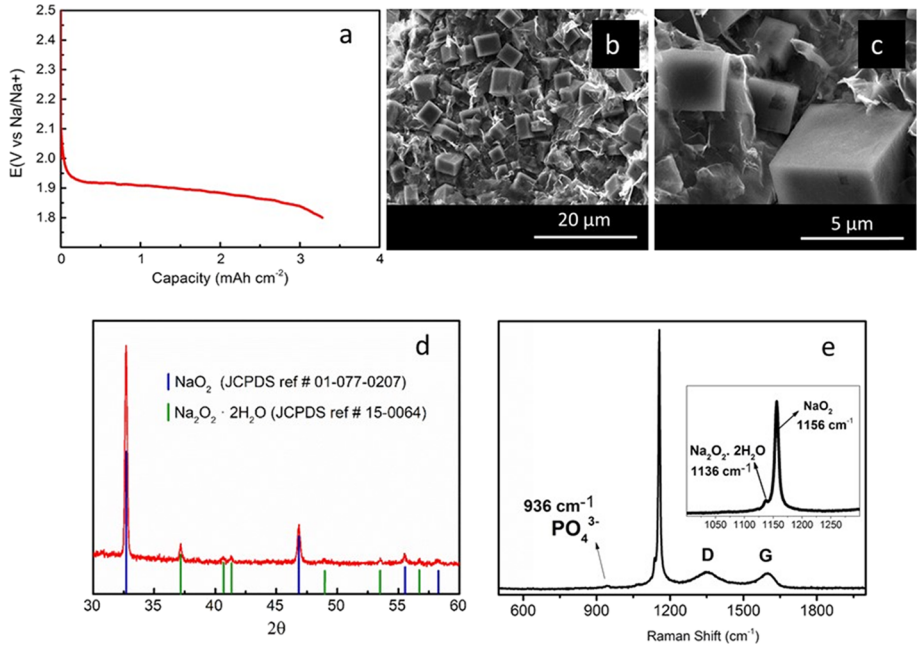

Figure 5. (a) Galvanostatic discharge to full capacity of the porous graphene aerogel cathode at 0.2 mA cm^{-2} using 0.1 M $NaPF_6$ in DEGDME. (b, c) SEM images, (d) XRD pattern, and (e) Raman spectrum of the discharged electrode.

flakes can be found in Figure S2 in the Supporting Information.

The chemical make-up of the graphene samples was ascertained by X-ray photoelectron spectroscopy (XPS). Figure 3e shows a representative high resolution C1s core-level spectrum (red trace), together with that of the starting graphite foil material (black trace) for comparison. Both were dominated by the graphitic component located at ∼284.6 eV (unoxidized sp^2-based C═C species). However, the graphene sample exhibited some additional components in the 286−289 eV binding energy range, which were attributed to the presence of both a certain fraction of strongly adsorbed nucleotide and carbon atoms oxidized during the anodic process (C−O, C═O species). Indeed, the strong adsorption of the nucleotides was confirmed by the detection of significant amounts of nitrogen and phosphorus in the survey XPS spectra of the samples (high-resolution N1s and P2p core level spectra are displayed in Figure S3 in the Supporting Information) even after extensive washing (up to 20 washing cycles). O/C atomic ratios for the graphenes obtained with the different nucleotides, which were derived from their corresponding survey XPS spectra taking into account the presence of adsorbed nucleotide (subtracting the oxygen and carbon coming from the adsorbed nucleotides), were ∼0.09 (compared to ∼0.01 for the starting graphite foil). These values were similar to those reported previously for anodic graphenes prepared with common, sulfate-based electrolytes,[2729,38,39,42] and indicated that the nanosheets carried a moderate extent of oxidation. The Raman spectra of the graphenes (Figure 3f, red trace) revealed the well-known graphitic G and defect-related D bands at 1582 and 1350 cm^{-1}, respectively. The integrated intensity ratio of the D and G bands (I_D/I_G ratio), a proxy for defect prevalence in graphite/graphene,[42] was typically 1.3−1.5, in agreement with prior data for moderately oxidized anodic graphenes[22,24,28,39,43] but much larger than that of the starting graphite foil (∼0.01; Figure 3f, black trace). Such an increase in the I_D/I_G ratio of the graphitic material upon exfoliation was mainly ascribed to lattice disorder brought about by the introduction of oxygen species in the nanosheets.[22]

2.2. Nucleotide-Based, Electrochemically Exfoliated Graphene Aerogel as a Cathode Material for Na-O_2

DOI: 10.1021/acsami.9b15509
ACS Appl. Mater. Interfaces 2020, 12, 494−506

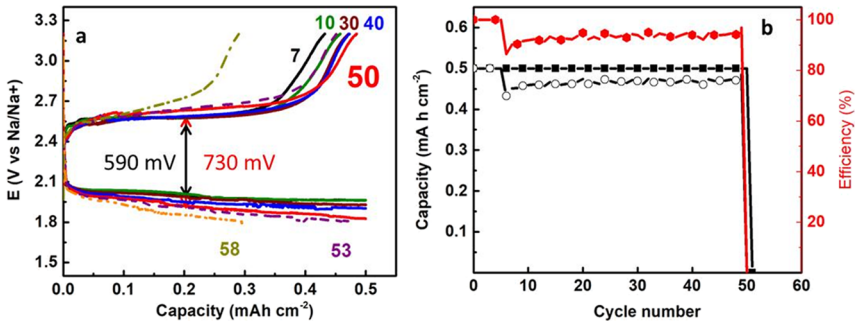

Figure 6. (a) Discharge and charge voltage profiles and (b) cycling behavior of Na−O_2 cells to a fixed capacity, with discharge capacity in black-filled square symbols, charge capacity in black-bared circular symbols, and coulombic efficiency in red-filled circular symbols.

Batteries. Graphene-based materials are promising candidates for their use as air cathodes in Na-O_2 batteries.[44,45] In this application, an open porous cathode architecture (e.g., a three-dimensional aerogel or foam) that enables a continuous supply of oxygen as well as suitable accommodation of the discharge products is crucial for the battery performance. Due to its high dispersibility in water and an oxygen-rich surface chemistry, GO is generally employed as a precursor in the preparation of three-dimensional graphene materials.[14,15,46,47] However, graphene nanosheets having low to moderate levels of oxidation have seldom been explored in such a context, probably as a result of their poor aqueous dispersibility. Still, the use of proper dispersing agents could open a window of opportunity for the fabrication of porous, three-dimensional architectures based on colloidal graphene nanosheets of limited oxidation that could be exploited. Here, anodic graphene obtained by the nucleotide-assisted electrochemical exfoliation and aqueous dispersion strategy described above was processed into free-standing, binder-free aerogels through a freeze-drying step (see the Experimental Section for details). Figure S4 in the Supporting Information shows digital photographs of as-prepared and smashed aerogels derived from the 0.1 M AMP dispersions from which circular electrode pieces were punched out. The porous structure of such electrodes was confirmed by both SEM imaging and N_2 physisorption (Figure 4). A platelet-like micrometer-scale morphology was observed in the SEM images (Figure 4a) with well-defined agglomerations of graphene nanosheets (~3.5 μm thickness). This difference with regard to STEM and AFM images displayed in Figure 3a−d is due to the film formation during the aerogel freeze-drying, as the structures shown Figure 4a are comprised of stacked graphene nanosheets. The aerogel displayed a type II isotherm (Figure 4b) with a negligible micropore contribution (BET specific surface area: 27 m^2 g^{-1}) and the presence of a certain amount of mesopores. The abrupt rise in the amount of adsorbed nitrogen at high relative pressures (>0.9) was indicative of large mesopores and macropores in the material, in agreement with the micrometer-/submicrometer-sized voids observed in the SEM images. The presence of 5−30 nm mesopores was revealed by the pore size distribution (PSD, Figure 4c), while the contribution of large pores was evaluated by helium pycnometry, yielding associated pore volumes of ~7.57 cm^3 g^{-1} and mean macropore size of ~2163 nm.

The graphene aerogel cathodes were electrochemically tested at a discharge current of 0.2 mA cm^{-2} using 0.1 M $NaPF_6$ in the diethylene glycol dimethyl ether (DEGDME) electrolyte. The cathodes delivered a full discharge capacity of 3.3 mAh cm^{-2} where a discharge plateau at 1.90 V is maintained up to 1.5 mAh cm^{-2} (Figure 5a). Homogeneously distributed cubes (~2.5−5 μm in size) were observed on the graphene aerogel surface by SEM (Figure 5b,c), suggesting the presence of NaO_2 as a discharge product.[48] It is important to note that the cubes formed in the present case were much smaller than those previously reported for graphene-derived air cathodes (typical sizes ~7−20 μm).[12,49] Likewise, the use of an alternative electrolyte (i.e., $NaPF_6$ in DEGDME instead of the more conventional $NaClO_4$ in DME) and/or the possible catalytic effect of the AMP molecules adsorbed on the anodic graphene nanosheets in the aerogel (discussed below) could also modify the nucleation behavior of the superoxide crystals. The preferential formation of the superoxide, as compared with other possible discharge products (Na_2O_2, Na_2O, or NaOH), is a highly desired feature because its redissolution during charge is kinetically favored.[7,50] Even though the formation of the superoxide is associated to a lower energy density in comparison to that afforded by the other discharge products, it generally leads to greater performance in terms of cyclability, which is currently the major handicap of this type of batteries. The X-ray diffraction (XRD) analysis of the as-discharged electrode revealed sodium superoxide formation as the main discharge product (NaO_2, JCPDS reference card no. 01-077-0207), while minor peaks related to Na_2O_2. $2H_2O$ (JCPDS reference card no. 15-0064) were also identified (Figure 5d). The presence of such an undesired product was also confirmed by Raman spectroscopy where a small shoulder at 1136 cm^{-1} can be observed together with an intense peak at 1156 cm^{-1} ascribed to NaO_2.[48] In addition, a very weak peak was identified at 936 cm^{-1} and assigned to phosphates belonging to the AMP molecules adsorbed on the cathode surface.[51] The formation of a small amount of hydrated sodium peroxide is believed to have arisen from the hydrophilic character that the AMP molecules confer to the graphene surface. Thus, higher drying temperatures for the cathode may be needed to remove the strongly adsorbed water molecules on the cathode surface.

The cyclic performance of the battery was examined by recording galvanostatic charge/discharge profiles at 0.2 mA cm^{-2} (Figure 6a) in shallow-cycling experiments[52] where the depth of discharge was limited to 0.5 mAh cm^{-2}. During the first few cycles, the cell suffered from voltage noise during charge (see Figure S5 in the Supporting Information). This behavior was believed to have arisen from the formation of the solid-electrolyte interphase (SEI)[53] or the existence of any passivation processes at the cathode. After these cycles, the cell stabilized and delivered 50 cycles with an efficiency of 95% (Figure 6b) before undergoing a gradual capacity fading. The latter was probably due to the accumulation of insoluble

DOI: 10.1021/acsami.9b15509
ACS Appl. Mater. Interfaces 2020, 12, 494−506

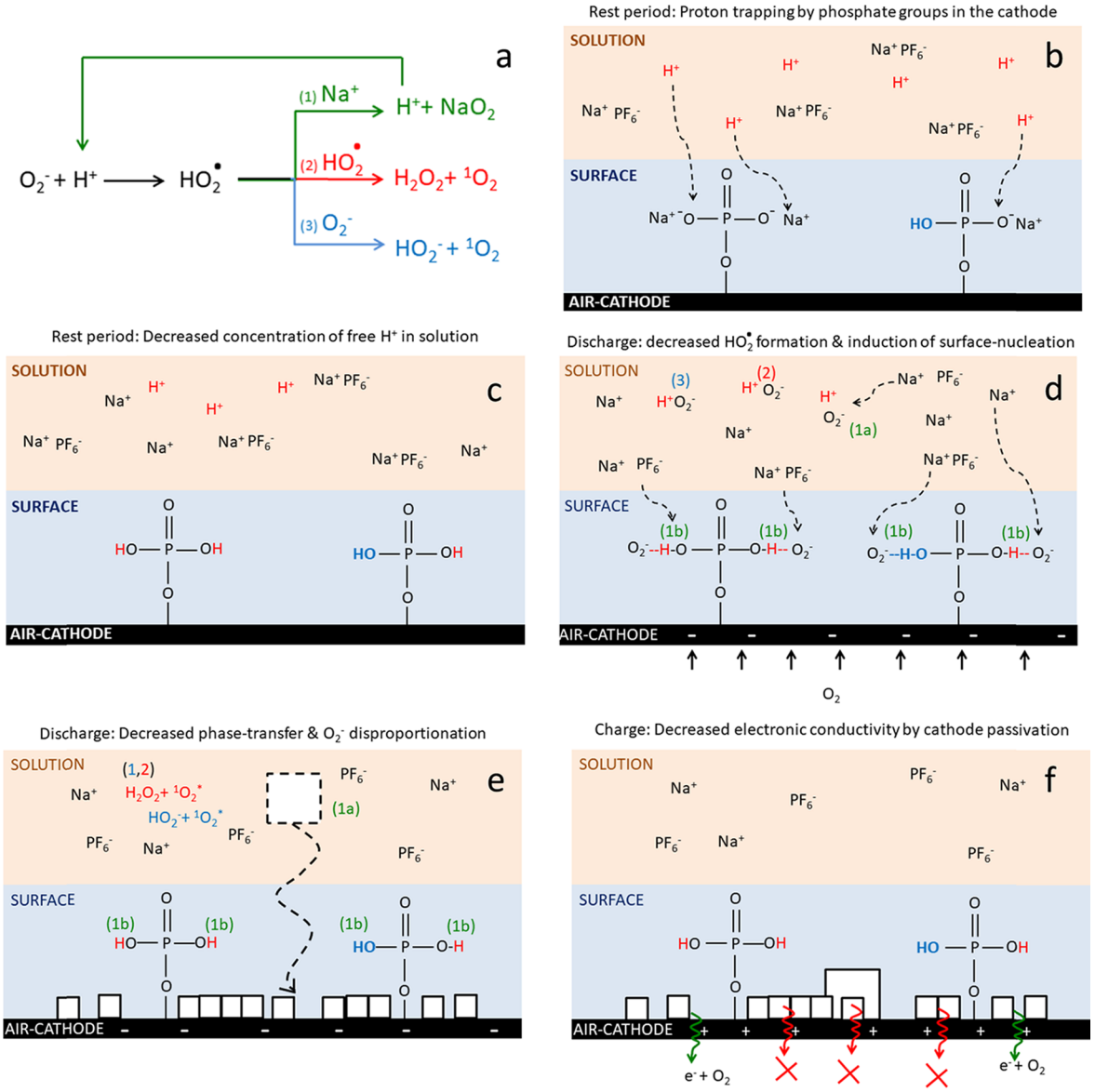

Figure 7. (a) Reactions occurring in a Na-O_2 battery during discharge and charge in the presence of protons. Proposed mechanisms occurring in the AMP-derived anodic graphene air-cathode during (b, c) resting period, (d) initial stages of discharge, (e) deeper discharge (cubes drawn in solid line represent surface-mediated mechanism and cubes in dotted line represent solution-mediated mechanism), and (f) charging step.

discharge products and pore clogging. This behavior is characteristic of metal-air batteries due to the passivation layer that saturates active sites in the cathode.[7] The flat shape of the charge−discharge curves suggested a favorable molecular diffusion and good homogeneity of the discharge products formed on both the pores and surface of the cathode. The cycling overpotential remained stable at ∼590 mV for the first 40 cycles but increased up to ∼730 mV during the last 10 cycles. Despite such a large overpotential, we note that the cyclability attained here (where metal-based catalyst or doping has not been used) was very competitive regarding the state of the art in graphene cathodes (performance results of current literature examples of Na-O_2 batteries with graphene-based cathodes are summarized in Table S1 in the Supporting Information).[12,49] Also, when compared with commonly used graphene-based cathodes, the aerogels prepared in this work offer the advantages of an environmentally friendly and nontoxic approach as well as the use of water as the only solvent during the preparation process. It is also important to note that the charge/discharge current applied here was higher than those commonly used, which is known to increase the cycling overpotential.[54] We hypothesize that the AMP molecules adsorbed on the graphene nanosheets favor the ORR reaction during discharge (Figure 5), but at the same time increase the charging overpotential by decreasing the electric conductivity of the aerogel electrode.

Figure 7a summarizes the main competitive reactions that take place during a Na-O_2 battery discharge in the presence of protons.[55] The reactive superoxide species (O_2^-), created during the oxygen reduction at the surface of the air cathode, react with protons coming from trace water and solvent. The resulting hydroperoxyl radicals ($HO_2^{\cdot}$) are soluble intermediates that transport the superoxide molecules from the cathode surface to the electrolyte phase. This stabilized superoxide reacts with Na^+ from the electrolyte to produce NaO_2. Even though a certain number of protons in the medium can

DOI: 10.1021/acsami.9b15509
ACS Appl. Mater. Interfaces 2020, 12, 494−506

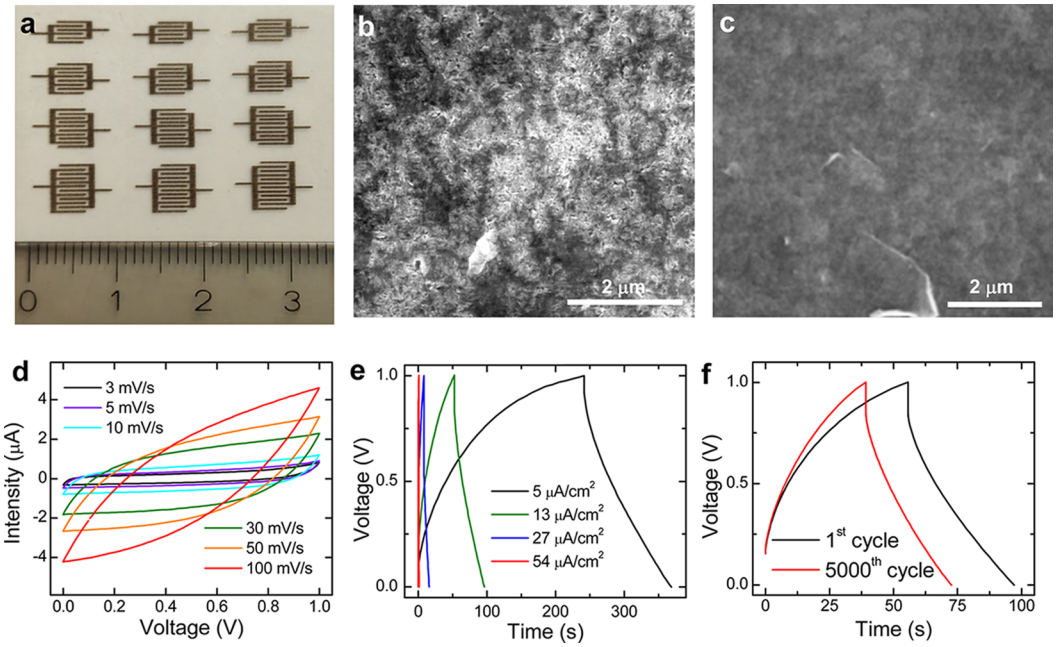

Figure 8. (a) Digital photograph of printed interdigitated graphene patterns. (b, c) Representative SEM micrographs of (b) the bare substrate (alumina-coated polyethylene terephthalate) and (c) the graphene pattern obtained after 30 print passes. Electrochemical testing of the interdigitated graphene patterns with PVA/H_2SO_4 gel (1:1 in weight) as the electrolyte: (d) cyclic voltammograms recorded at potential scan rates between 3 and 100 mV/s, (e) galvanostatic charge/discharge curves recorded at currents between 5 and 54 μA/cm^2, and (f) cyclability test for the microsupercapacitor at 5 μA/cm^2 for 5000 cycles. Ruler scale in (a) given in centimeters.

catalyze the formation of micrometer-sized and crystalline NaO_2 (reaction 1, Figure 7a), protons in excess can promote the formation of a large number of radicals that induce the disproportionation of O_2^- (reactions 2 and 3, Figure 7a). Hence, the hydroperoxyl radicals can react either with other hydroperoxyl radicals (reaction 2) or with other superoxide anions (reaction 3) to produce singlet oxygen ($^1O_2$), which is known to be the main driver for parasitic chemistry in metal-air batteries.[56] Regarding the formation of NaO_2, the presence of protons as a phase-transfer catalyst promotes a solution-mediated mechanism,[57,58] whereby the homogeneous nucleation of discharge products occurs in the bulk of the electrolyte. The random formation of nuclei in the electrolyte bulk and their migration thus favors growth of micrometer-sized NaO_2 particles that subsequently precipitate onto the cathode surface. On the other hand, the absence of hydroperoxyl radicals as phase-transfer mediators would lead to heterogeneous nucleation of the discharge products directly on the cathode surface (surface-mediated mechanism).[59,60] The latter mechanism is believed to produce amorphous and/or nanometer-sized NaO_2 cubes that decrease the cell performance. Hence, the formation of amorphous discharge products with small particle size will effectively passivate the cathode surface and hinder the electron transport.[61]

Bearing all this in mind, we hypothesize that the AMP molecules adsorbed on the anodic graphene nanosheets play a significant role, as they modify the chemistry involved in the charge/discharge process (Figure 7). Specifically, we note that the phosphate anions present in the AMP molecules, the pK_a values of which are around 3.9 and 6.1,[62] will just be partially protonated after preparation of the battery cathode from the aqueous, AMP-derived anodic graphene dispersion (the pH value of such a dispersion was measured to be ~6). After battery assembly and during the resting state (at open-circuit voltage, OCV), the nonprotonated oxygens from the AMP phosphate groups will bind the protons present in the electrolyte derived from trace water. This will lead to a decrease in the concentration of free protons in the bulk of the electrolyte prior to battery cycling (Figure 7b,c). During discharge, the oxygen reduced to O_2^- on the air-cathode will interact with either free protons from the electrolyte solution or with protons bound to the phosphate groups on the cathode surface (Figure 7d). The species interacting with free protons ($HO_2^{\cdot}$ intermediates) will favor the superoxide disproportionation to singlet oxygen (reactions 2 and 3 in Figure 7d) or the formation of micrometer-sized NaO_2 cubes by a solution-mediated mechanism (reaction 1a in Figure 7d). On the other hand, the superoxide molecules interacting with protonated phosphates would form an alternative acid intermediate (−C−PO_2−O−H−O_2^-, Figure 7d), which in turn would prompt the formation of nanometer-sized NaO_2 nuclei or even a film-like discharge layer by a surface-mediated mechanism (reaction 1b in Figure 7d). We therefore suggest that the phosphate groups in the AMP molecules act as (i) "proton scavengers" that reduce the proton-induced disproportionation of the superoxide molecules and (ii) catalytic/nucleation sites that promote the heterogeneous nucleation of discharge products directly on the cathode surface (Figure 7e). Such a mechanism would be consistent with the observation of relatively small-sized NaO_2 cubes on the discharged electrode (Figure 5b,d). Regarding the discharge state, an electrically insulating, passivation layer would be formed on the electrode surface, challenging the redissolution of the cubes and increasing the overpotential due to impeded electronic transport (Figure 7f). Such a conductivity decrease would also be consistent with the voltage noise observed during the first cycles of the battery operation (Figure S5) and the substantial charge overpotential (Figure 6a). Based on this knowledge, studies to reduce the cycling overpotential and avoid the uncontrollable formation of

DOI: 10.1021/acsami.9b15509
ACS Appl. Mater. Interfaces 2020, 12, 494−506

the solid-electrolyte interface during the first cycles are currently ongoing in our laboratory.

2.3. Inkjet-Printed Interdigitated Graphene Patterns as Electrodes for Microsupercapacitors. In recent years, graphene dispersions have attracted interest for their use as conductive inks for the direct printing of microsupercapacitors,[63,64] which have emerged as potential candidates to complement or even replace microbatteries. Unlike GO-based dispersions, graphene dispersions directly obtained through exfoliation from graphite, either by sonication or by electrochemical treatment, do not require any thermal or chemical treatment to remove oxides and make them electrically conductive, thus constituting a more straightforward and simple alternative. Furthermore, aqueous graphene dispersions, such as those prepared in this work with natural nucleotides, offer the additional advantage of environmental friendliness. The lateral dimensions of the present nanosheets (Figure 3a–d) made them appropriate for inkjet printing techniques, as they lied below the threshold for the nozzle blockage (2 μm).[65] On the basis of previously reported optimized printing protocols for graphene inks[66] (see the Experimental Section for details), interdigitated patterns with controllable and tunable geometry (Figure 8a) could be obtained with the present aqueous, nucleotide-assisted graphene dispersions. Since aqueous graphene dispersions were used, a common desktop printer designed for aqueous inks was employed for the printing. While most inkjet printers often used in research require additives to bring the Ohnesorge number into the printable range,[66] the printer used in this work was able to print patterns without any additives added to the inks, with electrode lateral sizes and separations below the millimeter range, and thicknesses in the range of hundreds of nanometers by means of several printing passes. A comparison between the typical SEM images of the bare alumina-coated polyethylene terephthalate (PET) substrate (Figure 8b) and the graphene patterns (Figure 8c) clearly showed that the surface of the substrate was covered by a smooth and continuous graphene film. The sharp, bright features observed in Figure 8c corresponded to the edges of some of the graphene flakes, which protruded slightly from the surface of the dried ink. To obtain functional microsupercapacitors, the surface of the graphene patterns was covered with a solid-state electrolyte (PVA/H_2SO_4 gel). The electrochemical performance of the devices in a two-electrode configuration was studied by cyclic voltammetry (CV) and galvanostatic charge/discharge (GCD) experiments with a potential window from 0.0 to 1.0 V. The results shown correspond to the pattern with three interdigitated microelectrodes. Figure 8d shows the CV curves measured at different scan rates from 3 to 100 mV s^{-1}. The quasi-rectangular shape of the CVs could in principle suggest a good capacitive behavior based on the formation of an electrical double layer. The absence of apparent redox peaks would confirm that faradaic reactions did not contribute to the charge storage process to a considerable extent.[67] However, a careful analysis of the CV curves was performed to make out and quantify capacitive and diffusion-controlled processes as reported in the literature.[68] This analysis indicated that the behavior of the printed devices was mostly due to pseudocapacitive, diffusion-controlled processes (~80%) and to a lesser extent to a capacitive behavior (~20%). This result was in good agreement with the morphology of the printed interdigitated patterns, which are comprised of restacked graphene nanosheets, and thus, the charge storage process can be expected to be dominated by the diffusion and intercalation of ions in the interlayer between neighboring nanosheets. Typical GCD curves recorded at different current densities between 5 and 54 μA cm^{-2} are shown in Figure 8e. The voltage drop at the beginning of each discharge curve, known as the IR drop, provided an indication of the overall resistance of the device (internal resistance), which was ~8×10^4 Ω. The device displayed values of areal capacitance, energy density, and power density of 0.27 mF cm^{-2}, 0.03 μW h cm^{-2}, and 0.003 mW cm^{-2}, respectively, at a current density of 5 μA cm^{-2}.

A comparison with the areal and volumetric capacitance, energy density, and power density values reported in the literature for graphene-based microsupercapacitors of similar electrode thickness (in the range from tenths of micron to a few microns) is gathered in Table S2 in the Supporting Information. These results were obtained at current densities in the same range as other reported devices, taking into account their respective electrode thicknesses. The devices prepared here exhibited a remarkable performance within the range of graphene-based printed microsupercapacitors (which display areal capacitances, energy densities, and power densities of 0.1–14.2 mF cm^{-2}, 0.005–3.92 μW h cm^{-2}, and 0.0001–152 mW cm^{-2}, respectively, at current densities of 0.014–20 μA cm^{-2}),[69,70] given that it performed similarly or better at higher current densities (direct comparison could be made in cases where the current density was known, the capacitance having been calculated from GCD data). As shown in Figure 8f, the device showed an acceptable cycling stability, retaining ~75% of the initial performance after 5000 charge/discharge cycles. Therefore, the devices shown in this work, printed from water-based graphene bio-ink, were functional and yielded competitive results when compared with other graphene-based printed devices of similar characteristics. It is important to note also that, different from the case of most printed graphene devices, which rely on inks that require complex and/or nonenvironmentally friendly processes (e.g., via the graphite oxide route or direct liquid phase exfoliation using organic solvents), the present approach displayed the alluring advantages of simplicity, nontoxicity, and environmental friendliness both in the preparation of the graphene inks as well as the printing of devices.

3. CONCLUSIONS

Graphene-based aerogels and inkjet-printed interdigitated patterns for use in Na-O_2 batteries and microsupercapacitors, respectively, were successfully obtained by resorting to a simple, all-aqueous, biomolecule-assisted, and integrated approach toward graphene exfoliation and processing. Taking advantage of the bifunctional character of natural nucleotides (e.g., adenosine monophosphate), which act efficiently both as an electrolyte for the electrochemical exfoliation of graphite and as a colloidal stabilizer for graphene dispersion, aqueous graphene bio-inks were attained in a streamlined process and used as a precursor for the fabrication of different electrode architectures (i.e., aerogels and interdigitated patterns). Na-O_2 batteries that relied on the graphene aerogels as the cathode and a glyme-containing electrolyte demonstrated an increased cycle life, a critical parameter in the development of this novel type of device, compared to previously reported batteries having graphene-based cathodes. A competitive performance was also achieved for microsupercapacitors assembled from the inkjet-printed graphene interdigitated electrodes but with the

DOI: 10.1021/acsami.9b15509
ACS Appl. Mater. Interfaces 2020, 12, 494–506

advantage of an electrode fabrication process that avoided the use of noninnocuous organic solvents and additives in the precursor ink. Finally, the present results suggest that combination of the graphene cathode with proper functional molecules could be a promising avenue in the efforts to improve the performance of metal-air batteries. Research along these lines is currently under way in our laboratory.

4. EXPERIMENTAL SECTION

4.1. Materials and Reagents. High-purity graphite foil (Papyex I980) was acquired from Mersen. Platinum foil, the nucleotides adenosine monophosphate (AMP), guanosine monophosphate (GMP), adenosine triphosphate (ATP), and flavin mononucleotide; the polymer poly(vinyl alcohol) (PVA, average molecular weight ~13−23 kDa); as well as concentrated H_2SO_4 (95−97%) were obtained from Sigma-Aldrich and used as received. Milli-Q deionized water (Millipore Corporation, resistivity: 18.2 MΩ·cm) was used in all the experiments.

4.2. Electrochemical Exfoliation and Colloidal Dispersion of Graphite in Aqueous Nucleotide Solutions. The electrochemical exfoliation experiments were accomplished in a two-electrode setup, using a rectangular piece of graphite foil (lateral dimensions: ~25 × 35 mm^2) as the anode, platinum foil (lateral dimensions: 25 × 25 mm) as the cathode, and an aqueous solution of a given nucleotide (AMP, GMP, ATP, or FMN) as the electrolytic medium. Different nucleotide concentrations in the 0.01−0.5 M range were tested, but optimum results were achieved at 0.05 M for ATP and 0.1 M for AMP and FMN and 0.2 M for GMP. The graphite and platinum foils were placed at a distance of about 2 cm from each other in the electrolytic cell and connected to an Agilent 6614C DC power supply. To induce expansion and delamination of the graphite electrode, a positive voltage of 10 V was applied to the latter for 60 min after which the expanded material was collected by gently scraping off the graphite foil with a spatula, transferred to the electrolytic solution, and bath-sonicated for 3 h (J.P. Selecta Ultrasons system, frequency: 40 kHz, power: ~22 W L^{-1}). The sonicated dispersion was then subjected to high-speed centrifugation (20,000 *g*, 20 min; Eppendorf 5424 microcentrifuge) to completely sediment the material, with the supernatant liquid (i.e., the remaining electrolytic solution) being removed and the sedimented product being redispersed in water through a brief (5−10 min) sonication step. The latter was finally submitted to low-speed centrifugation (200 *g*, 20 min) to remove the poorly exfoliated material (sediment) and obtain a dispersion of nucleotide-stabilized, anodically exfoliated graphene nanosheets (supernatant). The graphene concentration in these aqueous suspensions was estimated by means of UV−vis absorption spectroscopy, that is, making use of the Lambert−Beer law as reported elsewhere and measuring the absorbance at a wavelength of 660 nm (extinction coefficient, α_{660} = 2440 mL mg^{-1} m^{-1}).[32] To determine the reusability of electrolytes and graphite foil with a view to increase the overall efficiency of the graphene production process, the nucleotide solution and the scraped-off graphite foil remaining from a prior anodic exfoliation/dispersion experiment were both used in subsequent exfoliation/dispersion steps. It was observed that graphene products could still be obtained and suspended in water at least after four iterations.

4.3. Preparation of Graphene Aerogels and Inkjet-Printed Graphene Patterns. Graphene aerogels were prepared by direct freeze-drying of aqueous graphene suspensions prepared by anodic exfoliation and dispersion of graphite foil with 0.1 M AMP. To this end, 40 mL of 2 mg mL^{-1} graphene suspension was immersed in liquid nitrogen (−176 °C) and placed in a freeze-drier (Telstar LyoQuest apparatus) for 3 days. The resulting aerogel was smashed and cut into disc-shaped electrodes (0.95 cm^2). Interdigitated patterns consisting of 0.5 mm wide, 3.5 mm long fingers, separated by 0.5 mm gaps were printed with a Canon Pixma MG2550 inkjet printer using aqueous graphene dispersions prepared by electrochemical exfoliation of graphite foil with 0.1 M AMP as the ink. Experimental parameters such as the ink concentration, the printing substrate, and the total number of print passes were chosen on the basis of previous studies.[66] Specifically, the interdigitated patterns were printed on alumina-coated polyethylene terephthalate paper (Mitsubishi Paper Mills) after cleaning its surface with isopropyl alcohol and allowing it to dry. Graphene ink concentrations in the 1.5−2 mg mL^{-1} range were used, carrying out 30 print passes, and drying the patters between passes for 1 min in an oven at 55 °C. The thickness of the printed graphene film was derived from optical transmission data acquired with a transmission scanner as described elsewhere.[66] The resistance of the interdigitated patterns was measured by a two-point probe method, checking that there were no short circuits between microelectrodes.

4.4. Characterization Techniques. The different samples were analyzed by UV−vis absorption spectroscopy, scanning electron microscopy (SEM), scanning transmission electron microscopy (STEM), atomic force microscopy (AFM), X-ray photoelectron spectroscopy (XPS), Raman spectroscopy, nitrogen physisorption, helium pycnometry, and powder X-ray diffraction (XRD). UV−vis absorption spectra were recorded with a double-beam Helios α spectrophotometer (Thermo Spectronics). SEM images were obtained with either a Quanta 250 system or a Quanta 650 FEG (field emission gun) apparatus operated at 20 kV (FEI Company). The latter instrument was also used for STEM imaging. Graphene samples for STEM were prepared by mixing an aqueous graphene suspension with an equal volume of ethanol and then drop-casting 40 μL of the resulting water-ethanol dispersion onto a copper grid (200 mesh) covered with a thin film of amorphous carbon (Electron Microscopy Sciences), which was then allowed to dry under ambient conditions. AFM was accomplished with a Nanoscope IIIa Multimode apparatus working in the tapping mode of operation with rectangular silicon cantilevers (nominal spring constant: 40 N m^{-1}; resonance frequency: 250−300 kHz). Specimens for AFM were prepared by drop-casting a small volume (20−40 μL) of an aqueous graphene dispersion (~0.1 mg mL^{-1}) onto a SiO_2(300 nm)/Si substrate that was preheated at 50−60 °C and then allowed to dry. XPS measurements were carried out in a SPECS apparatus working at a pressure of 10^{-7} Pa with a monochromatic Al Kα X-ray source (14 kV, 175 W). Raman spectra were obtained on a Horiba Jobin-Yvon LabRam instrument with an excitation laser wavelength of 532 nm (green line) at an incident power of ~2.5 mW. To obtain accurate XPS data from the anodically exfoliated graphene, removing the nucleotide molecules adsorbed on the nanosheets was necessary. To this end, the aqueous nucleotide-stabilized graphene dispersions were subjected to repeated cycles of sedimentation via centrifugation (20,000 *g*, 20 min) and resuspension in water/isopropanol mixtures (65:35 v/v). The resulting dispersions were deposited dropwise onto preheated (50−60 °C) circular stainless steel sample holders until a uniform black film was seen to cover the whole substrate. The same XPS specimens were then used for Raman spectroscopy. Nitrogen physisorption at −196 °C was used to probe the micro/mesoporosity of the graphene aerogels with an ASAP 2020 apparatus (Micromeritics). Samples were degassed under a vacuum at 90 °C for 1 h and at 250 °C for 6 h. Pore size distribution (PSD) was determined by using a 2D-NLDFT heterogeneous surface method (equilibrium/desorption branch) and fitting with SAIEUS software. Aerogel macroporosity was examined by helium pycnometry with an AccuPyc II 1340 system (Micromeritics). PXRD was performed using a Bruker D8 Discover diffractometer with $\theta/2\theta$ Bragg−Brentano geometry (monochromatic Cu radiation: Kα_1 = 1.54056 Å) in the 30−60° range (2θ). For the morphological and structural characterization of the graphene aerogel electrodes after their discharge in the Na-O_2 battery, the electrodes were washed with fresh ethylene glycol dimethyl ether (DME) to remove the excess of conducting salt. The clean electrodes were subsequently transferred from an argon-filled glovebox to the SEM or PXRD instruments using an air-tight holder to avoid air exposure.

4.5. Cell Assembly and Electrochemical Characterization of Na-O_2 Batteries and Microsupercapacitors. For Na-O_2 batteries, a pressurized 2-electrode Swagelok-type cell (Figure S6) was used for the galvanostatic measurements. The cells were dried overnight at 120 °C and transferred to an argon-filled glovebox (H_2O < 0.1 ppm, O_2 <

DOI: 10.1021/acsami.9b15509
ACS Appl. Mater. Interfaces 2020, 12, 494−506

0.1 ppm; Jacomex, France) prior to the Na-O_2 cell assembly. The cells consisted of a disc-shaped sodium metal anode (0.95 cm^2, Sigma-Aldrich) and a graphene aerogel cathode (3.7−4.5 mg of graphene), sandwiching a Celgard H2010 membrane (Celgard USA, 1.33 cm^2) soaked in the electrolyte. The graphene electrodes were dried at 150 °C under a vacuum for 24 h and transferred to the glovebox without exposure to air. Anhydrous diethylene glycol dimethyl ether (DEGDME, Sigma-Aldrich) solvent and sodium hexafluorophospate ($NaPF_6$, 98%, Sigma-Aldrich) conductive salt were used to prepare the electrolyte (0.1 M $NaPF_6$ in DEGDME). DEGDME was dried over molecular sieves (3 Å, Sigma-Aldrich) for 1 week, and $NaPF_6$ was dried under a vacuum at 120 °C for 24 h before use. The electrolyte solution was prepared in the glovebox, and its final water content was below 20 ppm (determined by C20 Karl Fisher coulometer, Mettler Toledo). A 1.13 cm^2 stainless steel mesh (Alfa Aesar) was used as the current collector for the air cathode. Following assembly, the cells were pressurized with pure oxygen to ∼1 atm before the electrochemical measurements. The cells were allowed to rest at their open-circuit voltage (∼2.2−2.3 V vs Na^+/Na) for 8 h prior to applying current in a Bio-Logic SAS VSP potentiostat. The discharge and charge experiments were performed at a current density of 0.2 mA cm^{-2} with a potential cut-off between 1.8 and 3.2 V versus Na^+/Na.

To obtain a functional microsupercapacitor, a gel electrolyte of PVA/H_2SO_4 (1:1 in weight) was prepared by dissolving 1 g of H_2SO_4 and 1 g of PVA in 10 mL of water with the assistance of stirring and heat. The resulting solution was drop-casted on the graphene interdigitated pattern and allowed to dry overnight. To ensure good electrical contact, spots of the silver conductive ink (Alfa Aesar Liquid S-020) were used as contact points to clamp the two electrodes for the electrochemical tests. The electrochemical measurements were performed by means of a Biologic VSP potentiostat in a symmetrical two-electrode configuration. Both cyclic voltammograms at different potential scan rates and galvanostatic charge/discharge curves at different current densities were recorded. The capacitance, energy density, and power density were calculated according to the following equations

$$C = I\Delta t/\Delta V \quad (1)$$

$$E = {}^1/_2 C\Delta V^2 \quad (2)$$

$$P = E/\Delta t \quad (3)$$

where C (F) is the capacitance, I (A) is the discharge current, Δt (s) is the discharge time, ΔV (V) is the potential window after IR drop subtraction during discharge, E (W h) is the energy density, and P (W) is the power density. The areal capacitance, energy density, and power density were calculated as the corresponding magnitudes divided by the footprint area (area covered by the electrolyte), including interfinger gaps (0.165 cm^2), whereas the volumetric magnitudes were calculated by dividing into the effective volume of the device, which was obtained by multiplying its entire projected area by the thickness of the interdigitated graphene pattern (300 nm).

■ ASSOCIATED CONTENT

Supporting Information

The Supporting Information is available free of charge at https://pubs.acs.org/doi/10.1021/acsami.9b15509.

Digital photographs of graphene dispersions and aerogels, TEM images and XPS spectra of graphene nanosheets, galvanostatic cycling of Na-O_2 batteries, cell configuration schematics, and tables comparing battery and microsupercapacitor performances (PDF)

■ AUTHOR INFORMATION

Corresponding Authors

*E-mail: j.munuera@incar.csic.es (J.M.M.).

*E-mail: paredes@incar.csic.es (J.I.P.).

ORCID

Jose M. Munuera: 0000-0002-8176-4795
Juan I. Paredes: 0000-0002-0044-9153
Silvia Villar-Rodil: 0000-0002-5832-9971
Jonathan N. Coleman: 0000-0001-9659-9721
Teófilo Rojo: 0000-0003-2711-8458

Notes

The authors declare no competing financial interest.

■ ACKNOWLEDGMENTS

Funding by the Spanish Ministerio de Economía y Competitividad (MINECO) and the European Regional Development Fund (ERDF) through project MAT2015-69844-R and by the Spanish Ministerio de Ciencia, Innovación y Universidades, the Spanish Agencia Estatal de Investigación and ERDF through project RTI2018-100832-B-I00 is gratefully acknowledged. Partial funding by Plan de Ciencia, Tecnología e Innovación (PCTI) 2013-2017 del Principado de Asturias and the ERDF through project IDI/2018/000233 is also acknowledged. J.M.M. is grateful to the Spanish Ministerio de Educación, Cultura y Deporte (MECD) for his predoctoral contract (FPU14/00792). J.N.C. acknowledges the ERC Adv. Gr. FUTUREPRINT. This work was also financially supported by the European Union (Graphene Flagship, Core 2, grant number 785219). The authors thank Alaa Adawy for the scientific support at the laboratory of HR-TEM, Institute for Scientific and Technological Resources, University of Oviedo, Spain.

■ REFERENCES

(1) Zhu, J.; Yang, D.; Yin, Z.; Yan, Q.; Zhang, H. Graphene and Graphene-Based Materials for Energy Storage Applications. *Small* **2014**, *10*, 3480−3498.

(2) Raccichini, R.; Varzi, A.; Passerini, S.; Scrosati, B. The Role of Graphene for Electrochemical Energy Storage. *Nat. Mater.* **2015**, *14*, 271−279.

(3) Ji, L.; Meduri, P.; Agubra, V.; Xiao, X.; Alcoutlabi, M. Graphene-Based Nanocomposites for Energy Storage. *Adv. Energy Mater.* **2016**, *6*, 1502159.

(4) Wang, Z.; Gao, H.; Zhang, Q.; Liu, Y.; Chen, J.; Guo, Z. Recent Advances in 3D Graphene Architectures and their Composites for Energy Storage Applications. *Small* **2019**, *15*, 1803858.

(5) Liang, J.; Mondal, A. K.; Wang, D.-W.; Iacopi, F. Graphene-Based planar Microsupercapacitors: Recent Advances and Future Challenges. *Adv. Mater. Technol.* **2019**, *4*, 1800200.

(6) Kwabi, D. G.; Ortiz-Vitoriano, N.; Freunberger, S. A.; Chen, Y.; Imanishi, N.; Bruce, P. G.; Shao-Horn, Y. Materials Challenges in Rechargeable Lithium-Air Batteries. *MRS Bull.* **2014**, *39*, 443−452.

(7) Landa-Medrano, I.; Li, C.; Ortiz-Vitoriano, N.; Ruiz de Larramendi, I.; Carrasco, J.; Rojo, T. Sodium-Oxygen Battery: Steps Toward Reality. *J. Phys. Chem. Lett.* **2016**, *7*, 1161−1166.

(8) Ortiz-Vitoriano, N.; Drewett, N. E.; Gonzalo, E.; Rojo, T. High Performance Manganese-Based Layered Oxide Cathodes: Overcoming the Challenges of Sodium Ion Batteries. *Energy Environ. Sci.* **2017**, *10*, 1051−1074.

(9) Li, H.; Liang, J. Recent Development of Printed Micro-Supercapacitors: Printable Materials, Printing Technologies, and Perspectives. *Adv. Mater.* **2019**, *31*, 1805864.

(10) Kawamoto, M.; He, P.; Ito, Y. Green Processing of Carbon Nanomaterials. *Adv. Mater.* **2017**, *29*, 1602423.

(11) Paredes, J. I.; Villar-Rodil, S. Biomolecule-Assisted Exfoliation and Dispersion of Graphene and Other Two-Dimensional Materials: a Review of Recent Progress and Applications. *Nanoscale* **2016**, *8*, 15389−15413.

DOI: 10.1021/acsami.9b15509
ACS Appl. Mater. Interfaces 2020, 12, 494−506

(12) Enterría, M.; Botas, C.; Gómez-Urbano, J. L.; Acebedo, B.; López del Amo, J. M.; Carriazo, D.; Rojo, T.; Ortiz-Vitoriano, N. Pathways Towards High Performance Na−O_2 Batteries: Tailoring Graphene Aerogel Cathode Porosity & Nanostructure. *J. Mater. Chem. A* **2018**, *6*, 20778−20787.
(13) Chen, K.; Shi, L.; Zhang, Y.; Liu, Z. Scalable Chemical-Vapour-Deposition Growth of Three-Dimensional Graphene Materials Towards Energy-Related Applications. *Chem. Soc. Rev.* **2018**, *47*, 3018−3036.
(14) Wu, Y.; Zhu, J.; Huang, L. A Review of Three-Dimensional Graphene-Based Materials: Synthesis and Applications to Energy Conversion/Storage and Environment. *Carbon* **2019**, *143*, 610−640.
(15) Sherrell, P. C.; Mattevi, C. Mesoscale Design of Multifunctional 3D Graphene Networks. *Mater. Today* **2016**, *19*, 428−436.
(16) Bonaccorso, F.; Bartolotta, A.; Coleman, J. N.; Backes, C. 2D-Crystal-Based Functional inks. *Adv. Mater.* **2016**, *28*, 6136−6166.
(17) Niu, L.; Coleman, J. N.; Zhang, H.; Shin, H.; Chhowalla, M.; Zheng, Z. Production of Two-Dimensional Nanomaterials via Liquid-Based Direct Exfoliation. *Small* **2016**, *12*, 272−293.
(18) Abdelkader, A. M.; Cooper, A. J.; Dryfe, R. A. W.; Kinloch, I. A. How to Get Between the Sheets: a Review of Recent Works on the Electrochemical Exfoliation of Graphene Materials from Bulk Graphite. *Nanoscale* **2015**, *7*, 6944−6956.
(19) Yang, S.; Lohe, M. R.; Müllen, K.; Feng, X. New-Generation Graphene from Electrochemical Approaches: Production and Applications. *Adv. Mater.* **2016**, *28*, 6213−6221.
(20) Paredes, J. I.; Munuera, J. M. Recent Advances and Energy-Related Applications of High Quality/Chemically Doped Graphenes Obtained by Electrochemical Exfoliation Methods. *J. Mater. Chem. A* **2017**, *5*, 7228−7242.
(21) Yang, S.; Brüller, S.; Wu, Z.-S.; Liu, Z.; Parvez, K.; Dong, R.; Richard, F.; Samorì, P.; Feng, X.; Müllen, K. Organic Radical-Assisted Electrochemical Exfoliation for the Scalable Production of High-Quality Graphene. *J. Am. Chem. Soc.* **2015**, *137*, 13927−13932.
(22) Munuera, J. M.; Paredes, J. I.; Villar-Rodil, S.; Castro-Muñiz, A.; Martínez-Alonso, A.; Tascón, J. M. D. High Quality, Low-Oxidized Graphene via Anodic Exfoliation with table Salt as an Efficient Oxidation-Preventing co-Electrolyte for Water/Oil Remediation and Capacitive Energy Storage Applications. *Appl. Mater. Today* **2018**, *11*, 246−254.
(23) Pei, S.; Wei, Q.; Huang, K.; Cheng, H.-M.; Ren, W. Green Synthesis of Graphene Oxide by Seconds Timescale Water Electrolytic Oxidation. *Nat. Commun.* **2018**, *9*, 145.
(24) Munuera, J. M.; Paredes, J. I.; Villar-Rodil, S.; Ayán-Varela, M.; Martínez-Alonso, A.; Tascón, J. M. D. Electrolytic Exfoliation of Graphite in Water with Multifunctional Electrolytes: en route Towards High Quality, Oxide-Free Graphene Flakes. *Nanoscale* **2016**, *8*, 2982−2998.
(25) Feng, X.; Wang, X.; Cai, W.; Qiu, S.; Hu, Y.; Liew, K. M. Studies on Synthesis of Electrochemically Exfoliated Functionalized Graphene and Polylactic Acid/Ferric Phytate Functionalized Graphene Nanocomposites as New Fire Hazard Suppression Materials. *ACS Appl. Mater. Interfaces* **2016**, *8*, 25552−25562.
(26) Xia, Z. Y.; Pezzini, S.; Treossi, E.; Giambastiani, G.; Corticelli, F.; Morandi, V.; Zanelli, A.; Bellani, V.; Palermo, V. The Exfoliation of Graphene in Liquids by Electrochemical, Chemical, and Sonication-Assisted Techniques: a Nanoscale Study. *Adv. Funct. Mater.* **2013**, *23*, 4684−4693.
(27) Parvez, K.; Wu, Z.-S.; Li, R.; Liu, X.; Graf, R.; Feng, X.; Müllen, K. Exfoliation of Graphite into Graphene in Aqueous Solutions of Inorganic Salts. *J. Am. Chem. Soc.* **2014**, *136*, 6083−6091.
(28) Ambrosi, A.; Pumera, M. Electrochemically Exfoliated Graphene and Graphene Oxide for Energy Storage and Electrochemistry Applications. *Chem. − Eur. J.* **2016**, *22*, 153−159.
(29) Munuera, J. M.; Paredes, J. I.; Villar-Rodil, S.; Ayán-Varela, M.; Pagán, A.; Aznar-Cervantes, S. D.; Cenis, J. L.; Martínez-Alonso, A.; Tascón, J. M. D. High Quality, Low Oxygen Content and Biocompatible Graphene Nanosheets Obtained by Anodic Exfoliation of Different Graphite Types. *Carbon* **2015**, *94*, 729−739.
(30) Dewick, P. M. *Essentials of Organic Chemistry: for students of pharmacy, medicinal chemistry and biological chemistry*; John Wiley & Sons Ltd: Chichester, 2006, chapters 11 and 14.
(31) Ju, S.-Y.; Doll, J.; Sharma, I.; Papadimitrakopoulos, F. Selection of Carbon Nanotubes with Specific Chiralities using Helical Assemblies of Flavin Mononucleotide. *Nat. Nanotechnol.* **2008**, *3*, 356−362.
(32) Ayán-Varela, M.; Paredes, J. I.; Guardia, L.; Villar-Rodil, S.; Munuera, J. M.; Díaz-González, M.; Fernández-Sánchez, C.; Martínez-Alonso, A.; Tascón, J. M. D. Achieving Extremely Concentrated Aqueous Dispersions of Graphene Flakes and Catalytically Efficient Graphene-Metal Nanoparticle Hybrids with Flavin Mononucleotide as a High-Performance Stabilizer. *ACS Appl. Mater. Interfaces* **2015**, *7*, 10293−10307.
(33) Ossonon, B. D.; Bélanger, D. Functionalization of Graphene Sheets by the Diazonium Chemistry during Electrochemical Exfoliation of Graphite. *Carbon* **2017**, *111*, 83−93.
(34) Li, D.; Müller, M. B.; Gilje, S.; Kaner, R. B.; Wallace, G. G. Processable Aqueous Dispersions of Graphene Nanosheets. *Nat. Nanotechnol.* **2008**, *3*, 101−105.
(35) Seo, J.-W. T.; Green, A. A.; Antaris, A. L.; Hersam, M. C. High-Concentration Aqueous Dispersions of Graphene using Nonionic, Biocompatible Block Copolymers. *J. Phys. Chem. Lett.* **2011**, *2*, 1004−1008.
(36) Hammami, K.; El Feki, H.; Marsan, O.; Drouet, C. Adsorption of Nucleotides on Biomimetic Apatite: The Case of Adenosine 5′ Monophosphate (AMP). *Appl. Surf. Sci.* **2015**, *353*, 165−172.
(37) Alberty, R. A.; Smith, R. M.; Bockt, R. M. The Apparent Ionization Constants of the Adenosine Phosphates and Related Compounds. *J. Biol. Chem.* **1951**, *193*, 425−434.
(38) Huang, X.; Li, S.; Qi, Z.; Zhang, W.; Ye, W.; Fang, Y. Low Defect Concentration Few-Layer Graphene using a Two-Step Electrochemical Exfoliation. *Nanotechnology* **2015**, *26*, 105602.
(39) Lou, F.; Buan, M. E. M.; Muthuswamy, N.; Walmsley, J. C.; Rønning, M.; Chen, D. One-Step Electrochemical Synthesis of Tunable Nitrogen-Doped Graphene. *J. Mater. Chem. A* **2016**, *4*, 1233−1243.
(40) Nemes-Incze, P.; Osváth, Z.; Kámarás, K.; Biró, L. P. Anomalies in Thickness measurements of Graphene and Few Layer Graphite Crystals by Tapping Mode Atomic Force Microscopy. *Carbon* **2008**, *46*, 1435−1442.
(41) Solís-Fernández, P.; Paredes, J. I.; Villar-Rodil, S.; Martínez-Alonso, A.; Tascón, J. M. D. Determining the Thickness of Chemically Modified Graphenes by Scanning Probe Microscopy. *Carbon* **2010**, *48*, 2657−2660.
(42) Ferrari, A. C.; Basko, D. M. Raman Spectroscopy as a Versatile Tool for Studying the Properties of Graphene. *Nat. Nanotechnol.* **2013**, *8*, 235−246.
(43) Eredia, M.; Bertolazzi, S.; Leydecker, T.; El Garah, M.; Janica, I.; Melinte, G.; Ersen, O.; Ciesielski, A.; Samorì, P. Morphology and Electronic Properties of Electrochemically Exfoliated Graphene. *J. Phys. Chem. Lett.* **2017**, *8*, 3347−3355.
(44) Liu, W.; Sun, Q.; Yang, Y.; Xie, J.-Y.; Fu, Z.-W. An Enhanced Electrochemical Performance of a Sodium−Air Battery with Graphene Nanosheets as Air Electrode Catalysts. *Chem. Commun.* **2013**, *49*, 1951−1953.
(45) Li, Y.; Yadegari, H.; Li, X.; Banis, M. N.; Li, R.; Sun, X. Superior Catalytic Activity of Nitrogen-Doped Graphene Cathodes for High Energy Capacity Sodium−Air Batteries. *Chem. Commun.* **2013**, *49*, 11731−11733.
(46) Kim, J.-E.; Oh, J.-H.; Kotal, M.; Koratkar, N.; Oh, I.-K. Self-Assembly and Morphological Control of Three-Dimensional macroporous Architectures Built of Two-Dimensional Materials. *Nano Today* **2017**, *14*, 100−123.
(47) Wang, Z.-L.; Xu, D.; Xu, J.-J.; Zhang, L.-L.; Zhang, X.-B. Graphene Oxide Gel-Derived, Free-Standing, Hierarchically Porous Carbon for High-Capacity and High-Rate Rechargeable Li-O_2 Batteries. *Adv. Funct. Mater.* **2012**, *22*, 3699−3705.

DOI: 10.1021/acsami.9b15509
ACS Appl. Mater. Interfaces 2020, 12, 494−506

(48) Kim, J.; Park, H.; Lee, B.; Seong, W. M.; Lim, H.-D.; Bae, Y.; Kim, H.; Kim, W. K.; Ryu, K. H.; Kang, K. Dissolution and Ionization of Sodium Superoxide in Sodium-Oxygen Batteries. *Nat. Commun.* **2016**, *7*, 10670.
(49) Liu, T.; Kim, G.; Casford, M. T. L.; Grey, C. P. Mechanistic Insights into the Challenges of Cycling a Nonaqueous Na−O_2 Battery. *J. Phys. Chem. Lett.* **2016**, *7*, 4841−4846.
(50) Yadegari, H.; Sun, Q.; Sun, X. Sodium-Oxygen Batteries: a Comparative Review from Chemical and Electrochemical Fundamentals to Future Perspective. *Adv. Mater.* **2016**, *28*, 7065−7093.
(51) Fontana, M. D.; Mabrouk, K. B.; Kauffmann, T. H. *Spectroscopic Properties of Inorganic and Organometallic Compounds: Techniques, Materials and Applications*: RSC Publishing: Cambridge, 2013, Volume *44*, p. 40−67.
(52) Medenbach, L.; Bender, C. L.; Haas, R.; Mogwitz, B.; Pompe, C.; Adelhelm, P.; Schröder, D.; Janek, J. Origins of Dendrite Formation in Sodium−Oxygen Batteries and Possible Countermeasures. *Energy Technol.* **2017**, *5*, 2265−2274.
(53) Lutz, L.; Alves Dalla Corte, D.; Tang, M.; Salager, E.; Deschamps, M.; Grimaud, A.; Johnson, L.; Bruce, P. G.; Tarascon, J.-M. Role of Electrolyte Anions in the Na−O_2 Battery: Implications for NaO_2 Solvation and the Stability of the Sodium Solid Electrolyte Interphase in Glyme Ethers. *Chem. Mater.* **2017**, *29*, 6066−6075.
(54) Notten, P. H. L.; Bergveld, H. J.; Kruijt, W. S. *Battery Management Systems: Design by Modelling*: Springer Science & Business Media: Dordrecht, 2002, Chapter 6, p. 220.
(55) Schafzahl, L.; Mahne, N.; Schafzahl, B.; Wilkening, M.; Slugovc, C.; Borisov, S. M.; Freunberger, S. A. Singlet Oxygen during Cycling of the Aprotic Sodium-O_2 Battery. *Angew. Chem., Int. Ed.* **2017**, *56*, 15728−15732.
(56) Mahne, N.; Schafzahl, B.; Leypold, C.; Leypold, M.; Grumm, S.; Leitgeb, A.; Strohmeier, G. A.; Wilkening, M.; Fontaine, O.; Kramer, D.; Slugovc, C.; Borisov, S. M.; Freunberger, S. A. Singlet Oxygen Generation as a Major Cause for Parasitic Reactions during Cycling of Aprotic Lithium−Oxygen Batteries. *Nat. Energy* **2017**, *2*, 17036.
(57) Xia, C.; Black, R.; Fernandes, R.; Adams, B.; Nazar, L. F. The Critical Role of Phase-Transfer Catalysis in Aprotic Sodium Oxygen Batteries. *Nat. Chem.* **2015**, *7*, 496−501.
(58) Xia, C.; Fernandes, R.; Cho, F. H.; Sudhakar, N.; Buonacorsi, B.; Walker, S.; Xu, M.; Baugh, J.; Nazar, L. F. Direct Evidence of Solution-Mediated Superoxide Transport and Organic Radical Formation in Sodium-Oxygen Batteries. *J. Am. Chem. Soc.* **2016**, *138*, 11219−11226.
(59) Yadegari, H.; Sun, X. Recent Advances on Sodium-Oxygen Batteries: a Chemical Perspective. *Acc. Chem. Res.* **2018**, *51*, 1532−1540.
(60) Yadegari, H.; Franko, C. J.; Banis, M. N.; Sun, Q.; Li, R.; Goward, G. R.; Sun, X. How to Control the Discharge Products in Na-O_2 Cells: Direct Evidence Toward the Role of Functional Groups at the Air Electrode Surface. *J. Phys. Chem. Lett.* **2017**, *8*, 4794−4800.
(61) Galloway, T. A.; Dong, J.-C.; Li, J.-F.; Attard, G.; Hardwick, L. J. Oxygen Reactions on Pt{hkl} in a Non-Aqueous Na^+ Electrolyte: Site Selective Stabilisation of a Sodium Peroxy Species. *Chem. Sci.* **2019**, *10*, 2956−2964.
(62) Armarego, W. L. E.; Chai, C. L. L. *Purification of Laboratory Chemicals*: Butterworth/Heinemann (Elsevier Science), 5th Edition, 2003, p. 509.
(63) Kurra, N.; Jiang, Q.; Nayak, P.; Alshareef, H. N. Laser-Derived Graphene: A Three-Dimensional Printed Graphene Electrode and its Emerging Applications. *Nano Today* **2019**, *24*, 81−102.
(64) Wang, J.; Li, F.; Zhu, F.; Schmidt, O. G. Recent Progress in Micro-Supercapacitor Design, Integration, and Functionalization. *Small Methods* **2019**, *3*, 1800367.
(65) Torrisi, F.; Hasan, T.; Wu, W.; Sun, Z.; Lombardo, A.; Kulmala, T. S.; Hsieh, G.-W.; Jung, S.; Bonaccorso, F.; Paul, P. J.; Chu, D.; Ferrari, A. C. Inkjet-Printed Graphene Electronics. *ACS Nano* **2012**, *6*, 2992−3006.
(66) Finn, D. J.; Lotya, M.; Cunningham, G.; Smith, R. J.; McCloskey, D.; Donegan, J. F.; Coleman, J. N. Inkjet Deposition of Liquid-Exfoliated Graphene and MoS_2 Nanosheets for Printed Device Applications. *J. Mater. Chem. C* **2014**, *2*, 925−932.
(67) Gogotsi, Y.; Penner, R. M. Energy Storage in Nanomaterials − Capacitive, pseudocapacitive, or Battery-like? *ACS Nano* **2018**, *12*, 2081−2083.
(68) Noori, A.; El-Kady, M. F.; Rahmanifar, M. S.; Kaner, R. B.; Mousav, M. F. Towards Establishing Standard Performance Metrics for Batteries, Supercapacitors and Beyond. *Chem. Soc. Rev.* **2019**, *48*, 1272−1341.
(69) Zhou, F.; Huang, H.; Xiao, C.; Zheng, S.; Shi, X.; Qin, J.; Fu, Q.; Bao, X.; Feng, X.; Müllen, K.; Wu, Z.-S. Electrochemically Scalable Production of Fluorine-Modified Graphene for Flexible and High-Energy Ionogel-Based Microsupercapacitors. *J. Am. Chem. Soc.* **2018**, *140*, 8198−8205.
(70) Delekta, S. S.; Adolfsson, K. H.; Erdal, N. B.; Hakkarainen, M.; Östling, M.; Li, J. Fully inkjet Printed Ultrathin Microsupercapacitors Based on Graphene Electrodes and a Nano-Graphene Oxide Electrolyte. *Nanoscale* **2019**, *11*, 10172−10177.

DOI: 10.1021/acsami.9b15509
ACS Appl. Mater. Interfaces 2020, 12, 494−506